

## Wave propagation in functionally graded piezoelectric rods with rectangular cross-section

J. G. YU<sup>1,2)</sup>, B. ZHANG<sup>1)</sup>, J. E. LEFEBVRE<sup>3)</sup>, CH. ZHANG<sup>2)</sup>

<sup>1)</sup>*School of Mechanical and Power Engineering  
Henan Polytechnic University  
Jiaozuo 454003, China  
e-mail: yu@emails.bjut.edu.cn*

<sup>2)</sup>*Department of Civil Engineering  
University of Siegen  
D-57068 Siegen, Germany*

<sup>3)</sup>*University of Lille Nord de France, F-59000 Lille, France  
and  
UVHC, IEMN-DOAE, F-59313 Valenciennes Cedex 9, France  
and  
CNRS, UMR 8520, F-59650 Villeneuve d'Ascq, France*

FOR THE PURPOSE OF DESIGN AND OPTIMIZATION of functionally graded piezoelectric material (FGPM) transducers, wave propagation in FGPM structures has received much attention in the past twenty years. But research focused essentially on semi-infinite structures and one-dimensional structures, i.e., structures with a finite dimension in only one direction, such as horizontally infinite flat plates and axially infinite hollow cylinders. This paper proposes a double orthogonal polynomial series approach to solve the wave propagation problem in a two-dimensional (2D) FGPM structure, namely, an FGPM rod with a rectangular cross-section. The dispersion curves and electric potential distributions are illustrated.

**Key words:** wave propagation, rectangular rod, FGPM structures, double orthogonal polynomials, dispersion curves, electric potential distribution.

Copyright © 2015 by IPPT PAN

### 1. Introduction

COMPARED TO TRADITIONAL PIEZOELECTRIC MATERIAL transducers, functionally graded piezoelectric material (FGPM) transducers can avoid the incompatibilities that exist between the piezoelectric element and the host structure. i.e., structure under test, such as 1) the residual stress generated during the bonding process, 2) the interface defects and the possibility of interface crack growth, 3) severe stress jumps across the interface during high speed electrical actuation or mechanical loading and 4) disbonding resulted from temperature variation.

The advantages of FGPM have attracted many researchers to develop FGPM transducers by various methods [1–8].

For the purpose of design and optimization of FGPM transducers, many computational models were developed to solve the wave propagation in various FGPM structures in the past thirty years. The most frequently used are the various layered models. These models divide an FGM structure into a number of homogeneous or inhomogeneous thin layers, such as finite layer element [9], linearly inhomogeneous layer elements [10], quadratic inhomogeneous layer elements [11], finite elements [12], spectral element [13, 14] and versatile transfer matrix approach [15]. There are also some models that use FGM as continuous gradient medium, such as Wentzel–Kramer–Brillouin (WKB) method [16, 17], homotopy analysis method [18] and orthogonal polynomial series method [19, 20] and analytical solutions for SH waves [21].

So far, investigations on wave propagation in FGPM structures have focused essentially on semi-infinite structures and one-dimensional structures, i.e., structures with a finite dimension in only one direction, such as horizontally infinite flat plates and axially infinite hollow cylinders.

In practical applications, many piezoelectric elements have finite dimensions in two directions. One-dimensional models are not suitable for these structures. This paper proposes a double orthogonal polynomial series approach to solve wave propagation in a 2D FGPM structure: the FGPM rod with rectangular cross-section. Two cases are considered: the material gradient direction and the polarization direction, which are identical and orthogonal to each other, respectively. Dispersion curves and electric potential profiles of various rectangular FGPM rods are presented and discussed. In this paper, traction-free and open-circuit boundary conditions are assumed.

## 2. Mathematics and formulation of the problem

We consider an orthotropic piezoelectric rod with rectangular cross-section, which is infinite in wave propagating direction. Its width is  $d$  and its height is  $h$ , as shown in Fig. 1. Its polarizing direction is in the  $z$  direction. The origin of the Cartesian coordinate system is located at a corner of the rectangular cross-section and the rod lies in the positive  $y$ - $z$ -region, where the cross-section is defined by the region  $0 \leq z \leq h$  and  $0 \leq y \leq d$ .

For the wave propagation problem considered in this paper, the body forces and electric charges are assumed to be zero. Thus, the dynamic equations for the rectangular rod are governed by

$$(2.1) \quad T_{ij,j} = \rho \ddot{u}_i, \quad D_{i,i} = 0,$$

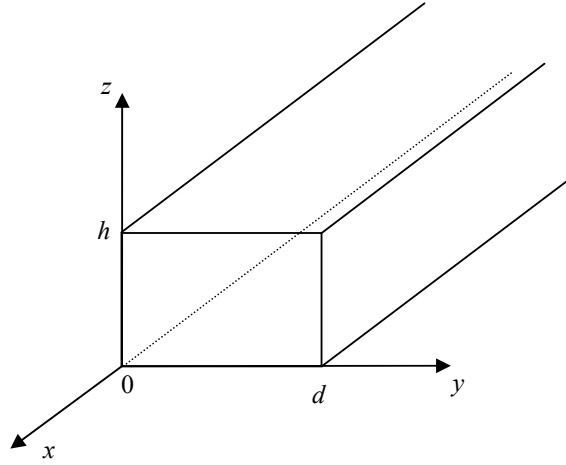


FIG. 1. Schematic diagram of a rod with rectangular cross-section.

where  $T_{ij}$ ,  $u_i$  and  $D_i$  are the stress, elastic displacement and electric displacement components, respectively;  $\rho$  is the density of the material.

The relationships between the strain and displacement components can be expressed as

$$(2.2) \quad \varepsilon_{ij} = 0.5(u_{i,j} + u_{j,i}), \quad E_i = -\phi_{,i},$$

where  $\varepsilon_{ij}$ ,  $E_i$  and  $\phi$  are the strain, electric field and electric potential components, respectively.

We introduce the function  $I(y, z)$

$$(2.3) \quad I(y, z) = \pi(y)\pi(z) = \begin{cases} 1, & 0 \leq y \leq d \text{ and } 0 \leq z \leq h, \\ 0, & \text{elsewhere,} \end{cases}$$

where  $\pi(y)$  and  $\pi(z)$  are rectangular window functions

$$\pi(y) = \begin{cases} 1, & 0 \leq y \leq d, \\ 0, & \text{elsewhere} \end{cases} \quad \text{and} \quad \pi(z) = \begin{cases} 1, & 0 \leq z \leq h, \\ 0, & \text{elsewhere.} \end{cases}$$

By introducing the function  $I(y, z)$ , the traction-free and open-circuit boundary conditions ( $T_{zz} = T_{xz} = T_{yz} = D_z = 0$  at  $z = 0$  and  $z = h$ , and  $T_{yy} = T_{xy} = T_{yz} = D_y = 0$  at  $y = 0$  and  $y = d$ ) are automatically incorporated in the constitutive relations of the plate [22]

$$(2.4) \quad \begin{aligned} T_{ij} &= (C_{ijkl}\varepsilon_{kl} - e_{kij}E_k)I(y, z), \\ D_j &= (e_{jkl}\varepsilon_{kl} + \epsilon_{jk}E_k)I(y, z) \end{aligned}$$

where  $C_{ij}$ ,  $e_{ij}$  and  $\epsilon_{ij}$  are the elastic, piezoelectric and dielectric coefficients respectively.

For the FGPM rod of material properties varying in the  $z$ -direction (we call it  $z$ -directional FGPM rod, the undermentioned FGPM rods are all  $z$ -directional FGM rods unless otherwise specified), the elastic parameters of the rod are functions of  $z$ , which can be expressed as

$$(2.5a) \quad C_{ijkl}(z) = \sum_{l=0}^L C_{ijkl}^{(l)} \left( \frac{z}{h} \right)^l.$$

Similarly, the other material coefficients can be represented by

$$(2.5b) \quad \begin{aligned} e_{kij}(z) &= \sum_{l=0}^L e_{kij}^{(l)} \left( \frac{z}{h} \right)^l, & \epsilon_{jk}(z) &= \sum_{l=0}^L \epsilon_{jk}^{(l)} \left( \frac{z}{h} \right)^l, \\ \rho(z) &= \sum_{l=0}^L \rho^{(l)} \left( \frac{z}{h} \right)^l, & l &= 0, 1, \dots, L. \end{aligned}$$

For the FGPM rod with material properties varying in the  $y$ -direction (we call it  $y$ -directional FGPM rod), the material parameters of the rod are functions of  $y$ , which can be expressed as

$$(2.6) \quad \begin{aligned} C_{ijkl}(y) &= \sum_{l=0}^L C_{ijkl}^{(l)} \left( \frac{y}{d} \right)^l, & e_{kij}(y) &= e_{kij}^{(l)} \left( \frac{y}{d} \right)^l, \\ \epsilon_{jk}(y) &= \epsilon_{jk}^{(l)} \left( \frac{y}{d} \right)^l, & \rho(y) &= \rho^{(l)} \left( \frac{y}{d} \right)^l, \quad l = 0, 1, \dots, L. \end{aligned}$$

For time-harmonic plane wave propagating in the  $x$ -direction of a rectangular rod, we assume that the displacement components have the following form:

$$(2.7a) \quad u_x(x, y, z, t) = \exp(ikx - i\omega t)U(y, z),$$

$$(2.7b) \quad u_y(x, y, z, t) = \exp(ikx - i\omega t)V(y, z),$$

$$(2.7c) \quad u_z(x, y, z, t) = \exp(ikx - i\omega t)W(y, z),$$

$$(2.7d) \quad \phi(x, y, z, t) = \exp(ikx - i\omega t)X(y, z),$$

where  $U(y, z)$ ,  $V(y, z)$  and  $W(y, z)$  represent the mechanical displacement amplitudes in the  $x$ -,  $y$ - and  $z$ -directions respectively, and  $X(y, z)$  represents the amplitude of electric potential,  $k$  is the magnitude of the wave vector in the propagation direction and  $\omega$  is the angular frequency.

Substituting Eqs. (2.2), (2.4), (2.5) or (2.6) and (2.7) into Eq. (2.1), the governing differential equations in terms of mechanical displacement and electric potential components can be obtained. Here, the case of identical material gradient and polarizing directions is given:

$$\begin{aligned}
 (2.8a) \quad & (z/h)^l [C_{55}^{(l)} U_{,zz} - k^2 C_{11}^{(l)} U + C_{66}^{(l)} U_{,yy} + ik(C_{12}^{(l)} + C_{66}^{(l)}) V_{,y} + ik(C_{13}^{(l)} + C_{55}^{(l)}) W_{,z} \\
 & + lz^{-1} C_{55}^{(l)} U_{,z} + ik(e_{15}^{(l)} + e_{31}^{(l)}) X_{,z} + lz^{-1} C_{55}^{(l)} W + likz^{-1} e_{15}^{(l)} X] I(y, z) \\
 & + (z/h)^l C_{66}^{(l)} (U_{,y} + ikV) I(y, z)_{,y} + (z/h)^l [C_{55}^{(l)} (U_{,z} + ikW) + ik e_{15}^{(l)} X] I(y, z)_{,z} \\
 & = -(z/h)^l \rho^{(l)} \omega^2 U \times I(y, z),
 \end{aligned}$$

$$\begin{aligned}
 (2.8b) \quad & (z/h)^l [C_{44}^{(l)} V_{,zz} - k^2 C_{66}^{(l)} V + ik(C_{12}^{(l)} + C_{66}^{(l)}) U_{,y} + (C_{23}^{(l)} + C_{44}^{(l)}) W_{,yz} \\
 & + lz^{-1} C_{44}^{(l)} (V_{,z} + W_{,y}) + C_{22}^{(l)} V_{,yy} + (e_{24}^{(l)} + e_{32}^{(l)}) X_{,yz} + lz^{-1} e_{24}^{(l)} X_{,y}] I(y, z) \\
 & + (z/h)^l [ikC_{12}^{(l)} U + C_{22}^{(l)} V_{,y} + C_{23}^{(l)} W_{,z} + e_{32}^{(l)} X_{,z}] I(y, z)_{,y} \\
 & + (z/h)^l [C_{44}^{(l)} (V_{,z} + W_{,y}) + e_{24}^{(l)} X_{,y}] I(y, z)_{,z} = -(z/h)^l \rho^{(l)} \omega^2 V \times I(y, z),
 \end{aligned}$$

$$\begin{aligned}
 (2.8c) \quad & (z/h)^l [C_{33}^{(l)} W_{,zz} - k^2 C_{55}^{(l)} W + C_{44}^{(l)} V_{,yy} + lz^{-1} (ikC_{13}^{(l)} U + C_{23}^{(l)} V_{,y} + C_{33}^{(l)} W_{,z}) \\
 & + ik(C_{13}^{(l)} + C_{55}^{(l)}) U_{,z} + (C_{23}^{(l)} + C_{44}^{(l)}) W_{,yz} + lz^{-1} e_{33}^{(l)} X_{,z} + e_{33}^{(l)} X_{,zz} + e_{24}^{(l)} X_{,yy} \\
 & - k^2 e_{15}^{(l)} x] I(y, z) + (z/h)^l [ikC_{13}^{(l)} U + C_{23}^{(l)} V_{,y} + C_{33}^{(l)} W_{,z} + e_{33}^{(l)} X_{,z}] I(y, z)_{,z} \\
 & + (z/h)^l [C_{44}^{(l)} (V_{,z} + W_{,y}) + e_{24}^{(l)} X_{,y}] I(y, z)_{,y} = -(z/h)^l \rho^{(l)} \omega^2 W \times I(y, z),
 \end{aligned}$$

$$\begin{aligned}
 (2.8d) \quad & (z/h)^l [ik(e_{31}^{(l)} + e_{15}^{(l)}) U_{,z} + ik(e_{24}^{(l)} + e_{32}^{(l)}) V_{,yz} + e_{33}^{(l)} W_{,zz} + e_{24}^{(l)} W_{,yy} - k^2 e_{15}^{(l)} W \\
 & - \epsilon_{33}^{(l)} X_{,zz} + k^2 \epsilon_{11}^{(l)} X - \epsilon_{22}^{(l)} X_{,yy} + lz^{-1} (e_{31}^{(l)} U + e_{32}^{(l)} V_{,y} + e_{33}^{(l)} W_{,z} + \epsilon_{33}^{(l)} X_{,z})] I(y, z) \\
 & + (z/h)^l (e_{24}^{(l)} V_{,z} + e_{24}^{(l)} W_{,y} - \epsilon_{22}^{(l)} X_{,y}) I(y, z)_{,y} \\
 & + (z/h)^l (ike_{31}^{(l)} U + e_{32}^{(l)} V_{,y} + e_{33}^{(l)} W_{,z} - \epsilon_{33}^{(l)} X_{,z}) I(y, z)_{,z} = 0,
 \end{aligned}$$

where subscript comma indicates partial derivative.

To solve the coupled wave equations (2.8),  $U(y, z)$ ,  $V(y, z)$ ,  $W(y, z)$  and  $X(y, z)$  are all expanded into products of two Legendre orthogonal polynomial series:

$$\begin{aligned}
 (2.9) \quad & U(y, z) = \sum_{m,j=0}^{\infty} p_{m,j}^1 Q_m(z) Q_j(y), \quad V(y, z) = \sum_{m,j=0}^{\infty} p_{m,j}^2 Q_m(z) Q_j(y), \\
 & W(y, z) = \sum_{m,j=0}^{\infty} p_{m,j}^3 Q_m(z) Q_j(y), \quad X(y, z) = \sum_{m,j=0}^{\infty} p_{m,j}^4 Q_m(z) Q_j(y),
 \end{aligned}$$

where  $p_{m,j}$  ( $i = 1, 2, 3, 4$ ) are the expansion coefficients and

$$(2.10) \quad \begin{aligned} Q_m(z) &= \sqrt{\frac{2m+1}{h}} P_m\left(\frac{2z-h}{h}\right), \\ Q_j(y) &= \sqrt{\frac{2j+1}{d}} P_j\left(\frac{2y-d}{d}\right) \end{aligned}$$

with  $P_m$  and  $P_j$  being the  $m$ th and the  $j$ th Legendre polynomials. Theoretically,  $m$  and  $j$  run from 0 to  $\infty$ . However, in practice the summation over the polynomials in Eq. (2.9) can be truncated at some finite values  $m = M$  and  $j = J$ , when the effects of higher order terms become negligible.

Equations (2.8) are multiplied by  $Q_n(z)$  with  $n$  running from 0 to  $M$ , and by  $Q_p(y)$  with  $p$  from 0 to  $J$ , respectively. Then integrating over  $z$  from 0 to  $h$  and over  $y$  from 0 to  $d$  gives the following system of linear algebraic equations:

$$(2.11a) \quad \begin{aligned} {}^l A_{11}^{n,p,m,j} p_{m,j}^1 + {}^l A_{12}^{n,p,m,j} p_{m,j}^2 + {}^l A_{13}^{n,p,m,j} p_{m,j}^3 + {}^l A_{14}^{n,p,m,j} p_{m,j}^4 \\ = -\omega^2 \cdot {}^l M_{n,p,m,j} p_{m,j}^1, \end{aligned}$$

$$(2.11b) \quad \begin{aligned} {}^l A_{21}^{n,p,m,j} p_{m,j}^1 + {}^l A_{22}^{n,p,m,j} p_{m,j}^2 + {}^l A_{23}^{n,p,m,j} p_{m,j}^3 + {}^l A_{24}^{n,p,m,j} p_{m,j}^4 \\ = -\omega^2 \cdot {}^l M_{n,p,m,j} p_{m,j}^2, \end{aligned}$$

$$(2.11c) \quad \begin{aligned} {}^l A_{31}^{n,p,m,j} p_{m,j}^1 + {}^l A_{32}^{n,p,m,j} p_{m,j}^2 + {}^l A_{33}^{n,p,m,j} p_{m,j}^3 + {}^l A_{34}^{n,p,m,j} p_{m,j}^4 \\ = -\omega^2 \cdot {}^l M_{n,p,m,j} p_{m,j}^3, \end{aligned}$$

$$(2.11d) \quad {}^l A_{41}^{n,p,m,j} p_{m,j}^1 + {}^l A_{42}^{n,p,m,j} p_{m,j}^2 + {}^l A_{43}^{n,p,m,j} p_{m,j}^3 + {}^l A_{44}^{n,p,m,j} p_{m,j}^4 = 0,$$

where  ${}^l A_{\alpha\beta}^{j,m}$  ( $\alpha, \beta = 1, 2, 3, 4$ ) and  ${}^l M_{m,j}$  are the elements of the nonsymmetric matrices  $\mathbf{A}$  and  $\mathbf{M}$ , which can be obtained by using Eq. (2.8).

Equation (2.11d) can be written as

$$(2.12) \quad p_{m,j}^4 = -({}^l A_{44}^{n,p,m,j})^{-1} ({}^l A_{41}^{n,p,m,j} p_{m,j}^1 + {}^l A_{42}^{n,p,m,j} p_{m,j}^2 + {}^l A_{43}^{n,p,m,j} p_{m,j}^3).$$

Substituting Eq. (2.12) into Eqs. (2.11a)–(2.11c) gives:

$$(2.13a) \quad \begin{aligned} [{}^l A_{11}^{n,p,m,j} - {}^l A_{14}^{n,p,m,j} ({}^l A_{44}^{n,p,m,j})^{-1} \cdot {}^l A_{41}^{n,p,m,j}] p_{m,j}^1 \\ + [{}^l A_{12}^{n,p,m,j} - {}^l A_{14}^{n,p,m,j} ({}^l A_{44}^{n,p,m,j})^{-1} \cdot {}^l A_{42}^{n,p,m,j}] p_{m,j}^2 \\ + [{}^l A_{13}^{n,p,m,j} - {}^l A_{14}^{n,p,m,j} ({}^l A_{44}^{n,p,m,j})^{-1} \cdot {}^l A_{43}^{n,p,m,j}] p_{m,j}^3 \\ = -\omega^{2l} M_{n,p,m,j} p_{m,j}^1, \end{aligned}$$

$$\begin{aligned}
 (2.13b) \quad & [{}^l A_{21}^{n,p,m,j} - {}^l A_{24}^{n,p,m,j} ({}^l A_{44}^{n,p,m,j})^{-1} \cdot {}^l A_{41}^{n,p,m,j}] p_{m,j}^1 \\
 & + [{}^l A_{22}^{n,p,m,j} - {}^l A_{24}^{n,p,m,j} ({}^l A_{44}^{n,p,m,j})^{-1} \cdot {}^l A_{42}^{n,p,m,j}] p_{m,j}^2 \\
 & + [{}^l A_{23}^{n,p,m,j} - {}^l A_{24}^{n,p,m,j} ({}^l A_{44}^{n,p,m,j})^{-1} \cdot {}^l A_{43}^{n,p,m,j}] p_{m,j}^3 \\
 & = -\omega^{2l} M_{n,p,m,j} p_{m,j}^2,
 \end{aligned}$$

$$\begin{aligned}
 (2.13c) \quad & [{}^l A_{31}^{n,p,m,j} - {}^l A_{34}^{n,p,m,j} ({}^l A_{44}^{n,p,m,j})^{-1} \cdot {}^l A_{41}^{n,p,m,j}] p_{m,j}^1 \\
 & + [{}^l A_{32}^{n,p,m,j} - {}^l A_{34}^{n,p,m,j} ({}^l A_{44}^{n,p,m,j})^{-1} \cdot {}^l A_{42}^{n,p,m,j}] p_{m,j}^2 \\
 & + [{}^l A_{33}^{n,p,m,j} - {}^l A_{34}^{n,p,m,j} ({}^l A_{44}^{n,p,m,j})^{-1} \cdot {}^l A_{43}^{n,p,m,j}] p_{m,j}^3 \\
 & = -\omega^{2l} M_{n,p,m,j} p_{m,j}^3.
 \end{aligned}$$

Then, Eqs. (2.11) can be rewritten as

$$\begin{aligned}
 (2.14) \quad & \begin{bmatrix} {}^l \bar{A}_{11}^{n,p,m,j} & {}^l \bar{A}_{12}^{n,p,m,j} & {}^l \bar{A}_{13}^{n,p,m,j} \\ {}^l \bar{A}_{21}^{n,p,m,j} & {}^l \bar{A}_{22}^{n,p,m,j} & {}^l \bar{A}_{23}^{n,p,m,j} \\ {}^l \bar{A}_{31}^{n,p,m,j} & {}^l \bar{A}_{32}^{n,p,m,j} & {}^l \bar{A}_{33}^{n,p,m,j} \end{bmatrix} \begin{Bmatrix} p_{m,j}^1 \\ p_{m,j}^2 \\ p_{m,j}^3 \end{Bmatrix} \\
 & = -\omega^{2l} M_{n,p,m,j} \begin{bmatrix} 1 & 0 & 0 \\ 0 & 1 & 0 \\ 0 & 0 & 1 \end{bmatrix} \begin{Bmatrix} p_{m,j}^1 \\ p_{m,j}^2 \\ p_{m,j}^3 \end{Bmatrix}.
 \end{aligned}$$

Thus, Eq. (2.14) forms the eigenvalue problem to be solved. The eigenvalue  $\omega^2$  is the angular frequency of the guided wave, and the eigenvectors  $p_{m,j}^i$  ( $i = 1, 2, 3, 4$ ) are the mechanical displacement components to be calculated. In terms of Eq. (2.12),  $p_{m,j}^4$  can be obtained, which determines the electric potential distribution. According to the equation  $Vph = \omega/k$ , the phase velocity can be obtained. In the computing progress, the obtained eigenvalues are complex, but their imaginary parts are all very small compared to their corresponding real parts. For one eigenvalue, its imaginary part is less than one-millionth of its real part. So, we just assume that the real parts are solutions of the system.

### 3. Numerical results and discussions

The Voigt-type model is used in this study to calculate the effective parameters of the FGM rod, which can be expressed as

$$(3.1a) \quad C(z) = C_1 V_1(z) + C_2 V_2(z), \quad \text{for } z\text{-directional FGM rectangular rod,}$$

$$(3.1b) \quad C(y) = C_1 V_1(y) + C_2 V_2(y), \quad \text{for } y\text{-directional FGM rectangular rod,}$$

where  $V_i(z)$  and  $C_i$  denote the volume fraction of the  $i$ th material and the cor-

responding physical property of the  $i$ th material, respectively, and  $\sum V_i(z) = 1$ . Thus, the properties of the FGM can be expressed as

$$(3.2a) \quad C(z) = C_2 + (C_1 - C_2)V_1(z), \quad \text{for } z\text{-directional FGM rectangular rod,}$$

$$(3.2b) \quad C(y) = C_2 + (C_1 - C_2)V_1(y), \quad \text{for } y\text{-directional FGM rectangular rod,}$$

According to Eqs. (2.5) and (2.6), the gradient profile of the material volume fraction can be expressed as a power series expansion. The coefficients of the power series can be determined using the Mathematica function ‘Fit’.

### 3.1. Comparison with the available solution from the semi-analytical finite element method

Because no reference results for the guided waves in rectangular FGPM rods can be found in literature, we consider a square homogeneous steel rod with  $C_L = 5.85$  km/s,  $C_T = 3.23$  km/s and  $h = d = 5.08$  mm to make a comparison with known results from the semi-analytical finite element method [23]. Here,  $C_L$  and  $C_T$  are respectively the longitudinal and transversal wave velocities. Figure 2 shows the corresponding dispersion curves, where dotted lines are from HAYASHI *et al.* [23], and solid red lines are obtained from the present extended polynomial approach. As can be seen, the results from the extended polynomial approach agree well with the reference data, which supports the correctness and the accuracy of the present method.

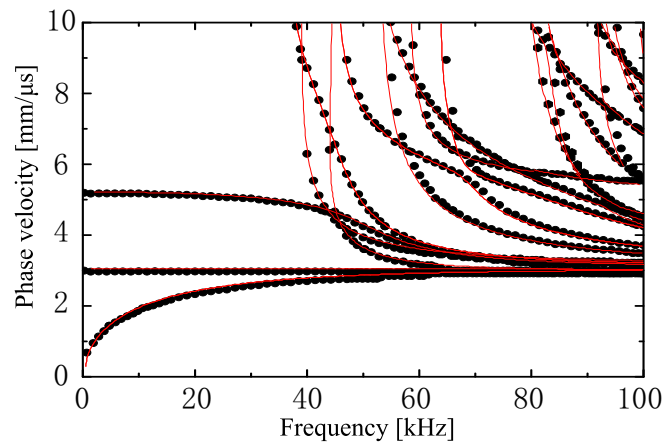


FIG. 2. Phase velocity dispersion curves for the steel square rod; dotted lines: results from the semi-analytical finite element method [23], solid red lines: the authors' results.

### 3.2. Dispersion curves in rectangular FGPM rods

In this section, we take the rectangular PZT-4-BSN FGPM rod as an example to discuss the wave characteristics. The FGPM rod is composed of PZT-4 (bottom surface) and BSN and the corresponding material parameters are given in Table 1. Firstly, we consider three square FGPM rods. Their respective gradient functions are linear, quadratic and cubic functions, i.e.,  $V_1(z) = z^n$  ( $n = 1, 2$  and  $3$ ). Their velocity dispersion curves are shown in Fig. 3. It can be observed that the first four wave modes have no cut-off frequencies. This feature is different from that for an infinite FGPM flat plate, in which the first three modes have no cut-off frequencies. Furthermore, different gradient varieties result in different dispersive characteristics. The wave speed of linearly graded rod is higher than that of quadratically and cubically graded rods. This is attributable to the fact that the volume fraction of PZT-4 in linearly graded rod is lower than that in other two graded rods and the bulk wave speed of PZT-4 is lower than that of BSN.

**Table 1. Physical parameters of the two piezoelectric materials.**

Property	$C_{11}$	$C_{12}$	$C_{13}$	$C_{22}$	$C_{23}$	$C_{33}$	$C_{44}$	$C_{55}$	$C_{66}$
PZT-4	13.9	7.4	7.4	13.9	7.4	11.5	2.56	2.56	3.05
BSN	23.9	10.4	5	24.7	5.2	13.5	6.5	6.6	7.6
	$e_{15}$	$e_{24}$	$e_{31}$	$e_{32}$	$e_{33}$	$\varepsilon_{11}$	$\varepsilon_{22}$	$\varepsilon_{33}$	$\rho$
PZT-4	12.7	12.7	-5.2	-5.2	15.1	650	650	560	7.5
BSN	2.8	3.4	-0.4	-0.3	4.3	196	201	28	5.3

Units:  $C_{ij}$  ( $10^{10}$  N/m<sup>2</sup>),  $\varepsilon_{ij}$  ( $10^{-11}$  F/m),  $e_{ij}$  (C/m<sup>2</sup>),  $\rho$  ( $10^3$  kg/m<sup>3</sup>).

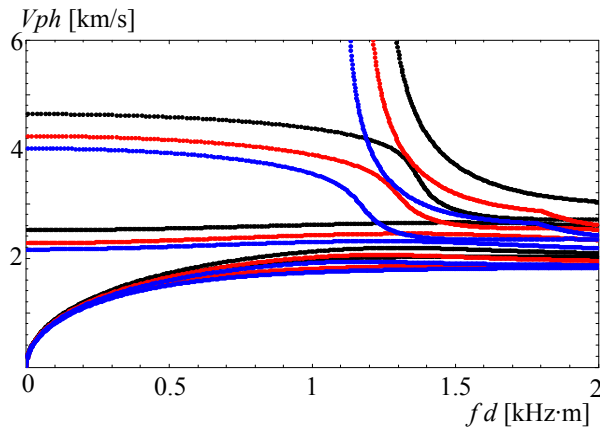


FIG. 3. Phase velocity dispersion curves for FGPM square rods; black lines: linearly graded rod, red lines: quadratically graded rod, blue lines: cubically graded rod.

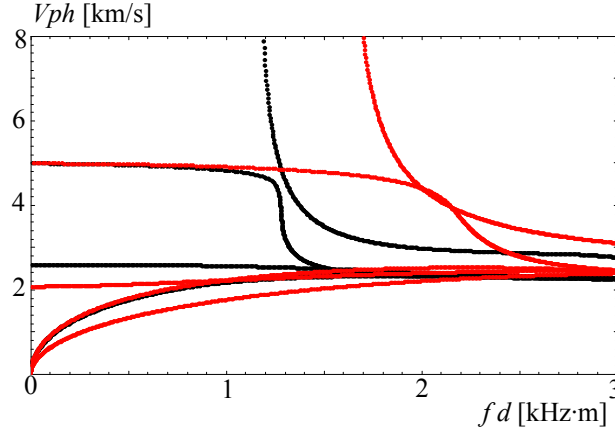


FIG. 4. Phase velocity dispersion curve for sinusoidally FGPM rectangular rods; black lines: with  $d/h = 1$ , red lines: with  $d/h = 2$ .

The gradient fields of above two FGPM rods are monotonic. Next, two sinusoidally FGPM rods ( $V_1(z) = \sin(\pi z)$ ) with different width to height ratio  $d/h = 1$  and  $d/h = 2$  are considered. The corresponding phase velocity dispersion curves are shown in Fig. 4. It can be seen that the width to height ratio has a significant influence on the dispersion curves. For the sinusoidally FGPM square rod, its geometric shape and material distribution are both symmetric with respect to both  $z$ - and  $y$ -axis. The first two modes are almost overlapped and the third mode is almost not dispersive. For the sinusoidally FGPM rectangular rod, its geometric shape is not symmetric with respect to  $z$ - and  $y$ -axis. The first two modes are not overlapped and the third mode is obviously dispersive. But it has the same material distribution like the square FGPM rod, which results in phase velocities similar to the ones of the square rod; as the width increases, the frequency of each mode becomes higher.

### 3.3. Mechanical displacement and electric potential distributions

Firstly, the distributions of the first four modes for sinusoidally FGPM square rod are shown in Figs. 5–8 at  $kd = 3$ . Because this structure is symmetric with respect to the geometry and the material distribution, its mechanical displacement and electric potential are all symmetric or anti-symmetric with respect to both  $y$  and  $z$  variables. For the first mode, Fig. 5, the distribution of the mechanical displacement component  $u$  is symmetric with respect to the  $z$  variable but antisymmetric with respect to the  $y$  variable. The other two mechanical displacement components  $v$  and  $w$  are respectively symmetric and antisymmetric

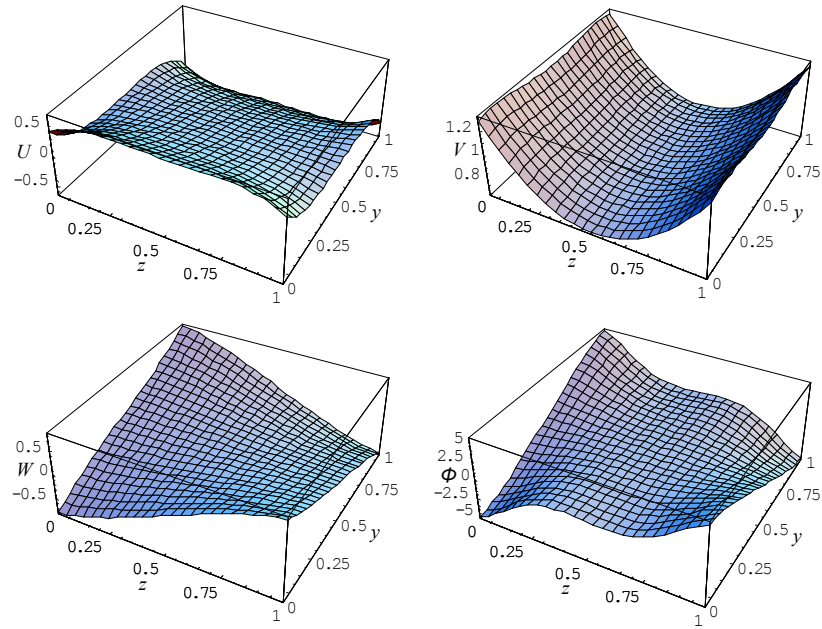


FIG. 5. Displacement and electric potential profiles of the first mode for the sinusoidally FGPM square rod at  $kd = 3$ .

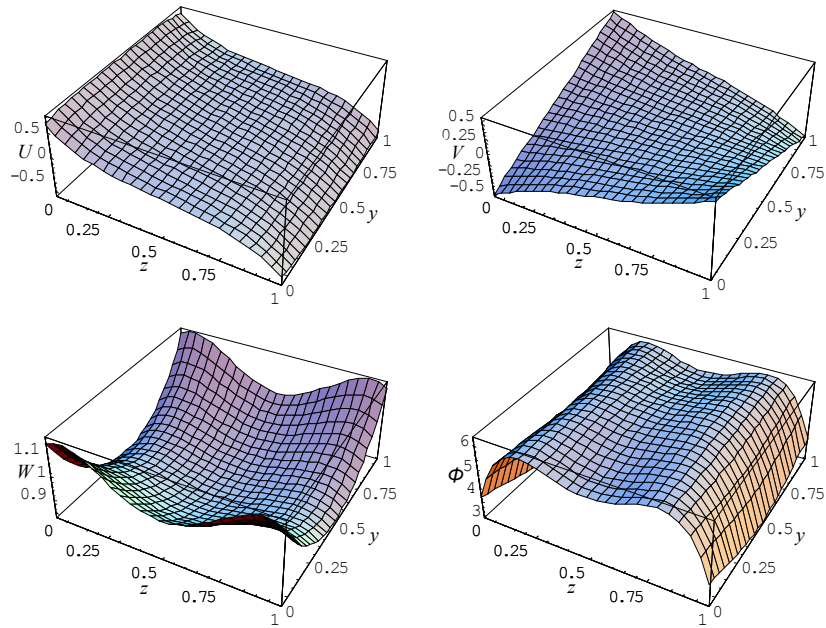


FIG. 6. Displacement and electric potential profiles of the second mode for the sinusoidally FGPM square rod at  $kd = 3$ .

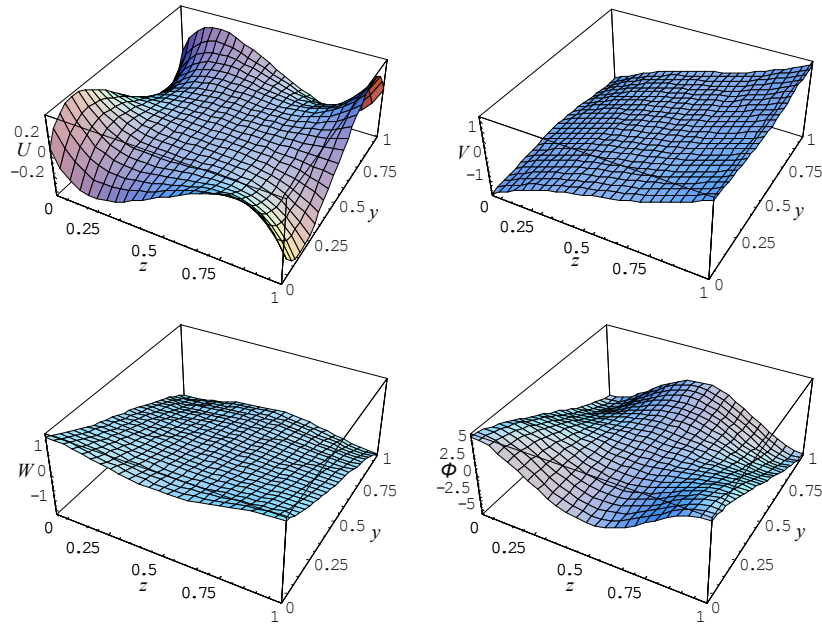


FIG. 7. Displacement and electric potential profiles of the third mode for the sinusoidally FGPM square rod at  $kd = 3$ .

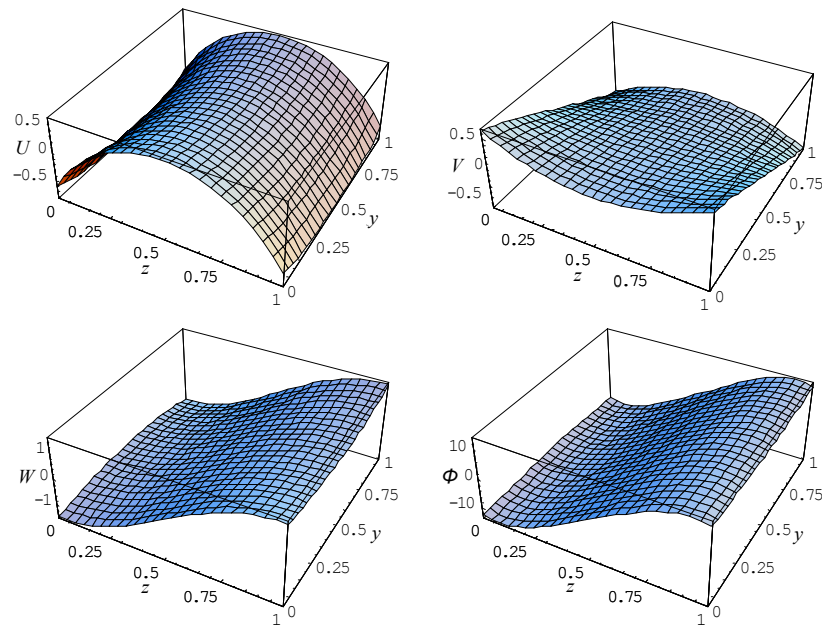


FIG. 8. Displacement and electric potential profiles of the fourth mode for the sinusoidally FGPM square rod at  $kd = 3$ .

with respect to both  $z$ - and  $y$ -axis. The mechanical displacement distribution of the second mode, Fig. 6, is the reverse of that of the first mode. Its mechanical displacement  $u$  is antisymmetric with respect to the  $z$  variable but symmetric with respect to the  $y$  variable. The mechanical displacement components  $v$  and  $w$  are respectively antisymmetric and symmetric with respect to both  $z$  and  $y$  variables. Furthermore, the mechanical displacement amplitudes of the first two modes are very similar: the amplitudes of displacement  $u$  are almost equal and the amplitudes of displacements  $v$  and  $w$  for the first mode are very close to those of  $v$  and  $w$  for the second mode. Similar comments can be made for the mechanical displacement components of the third mode, Fig. 7, and the fourth mode, Fig. 8. The electric potential of all modes has the same symmetry as the corresponding mechanical displacement  $w$ .

Then, Figs. 9 and 10 show the mechanical displacement and electric potential distributions of the first two modes for the linearly FGPM square rod at  $kd = 3$ . This rod is symmetric only with respect to the geometry but not to the material distribution. Its mechanical displacement components and electric potential are always symmetric or antisymmetric with respect to the  $y$  variable but not to the  $z$  one.

Next, the case of large wavenumber is discussed. Figures 11–14 are the displacement and electric potential distributions of the first and third modes for the sinusoidally and linearly FGPM square rods at  $kd = 60$ . It can be observed that the mechanical displacement and electric potential always distribute near the four boundaries. Furthermore, they mostly distribute in the dominantly PZT-4 regions (the wave speed of PZT-4 is lower than that of BSN). For example, in the sinusoidally FGPM rod, they mostly distribute near  $z = 0$  and  $z = 1$  and in the linearly FGPM rod near  $z = 0$ .

### 3.4. The case of $y$ -directional FGPM rod

This section considers a linearly  $y$ -directional FGPM square rod. Its phase velocity dispersion curves are shown in Fig. 15. Comparing them with those of Fig. 3a, it can be seen that although the geometric dimensions, material volume fractions and material gradient pattern are all the same, the different gradient direction results in different dispersion characteristics. In fact, the only constant factor is the polarization direction. This constant polarization direction and the changed gradient direction result in the difference of the two FGPM rods. Figure 16 presents the mechanical displacement components and electric potential distributions of the third mode at  $kd = 60$ . We can see again that the mechanical displacement and electric potential are always distributed dominantly in the PZT-4 region.

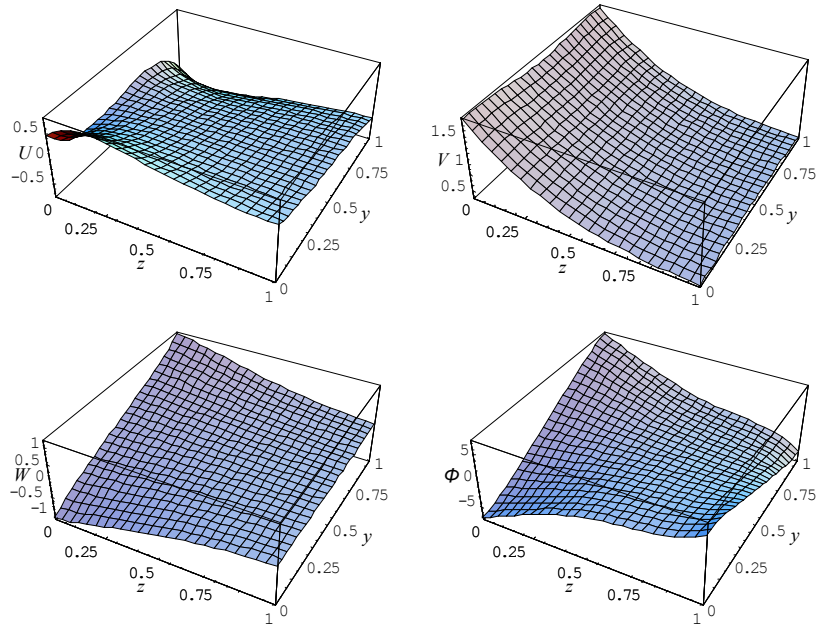


FIG. 9. Displacement and electric potential profiles of the first mode for the linearly FGPM square rod at  $kd = 3$ .

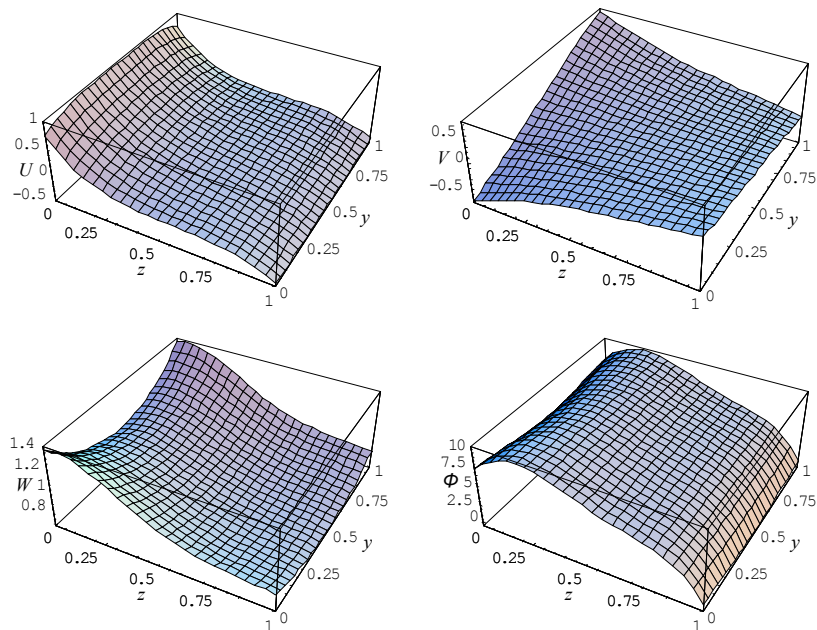


FIG. 10. Displacement and electric potential profiles of the second mode for the linearly FGPM square rod at  $kd = 3$ .

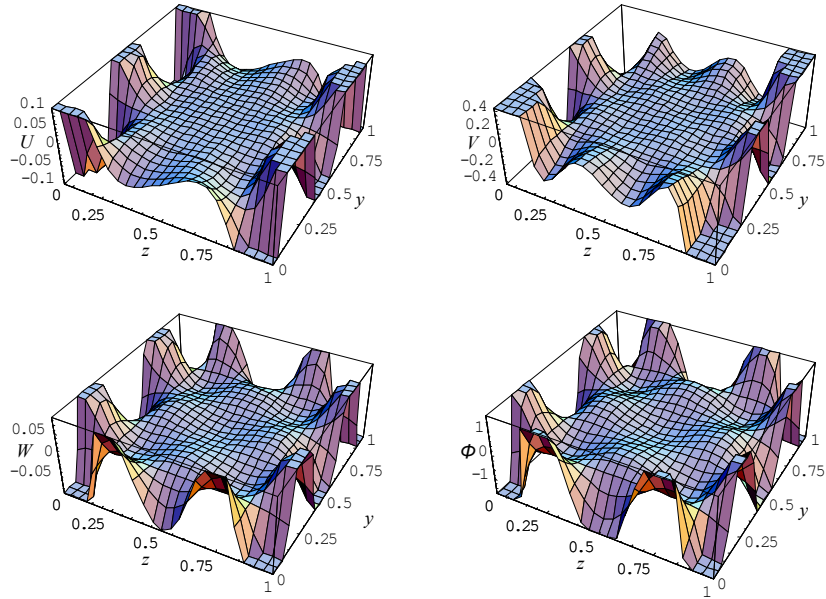


FIG. 11. Displacement and electric potential profiles of the first mode for the sinusoidally FGPM square rod at  $kd = 60$ .

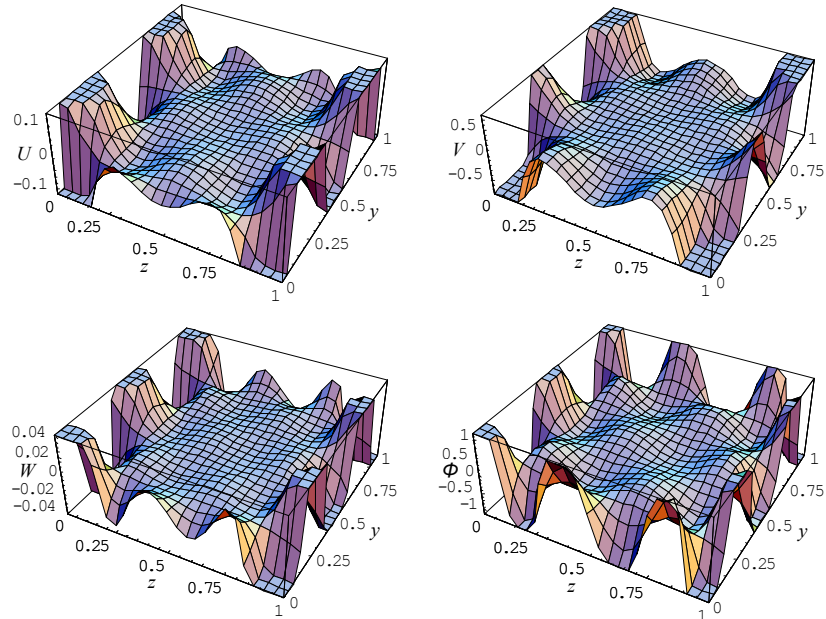


FIG. 12. Displacement and electric potential profiles of the third mode for the sinusoidally FGPM square rod at  $kd = 60$ .

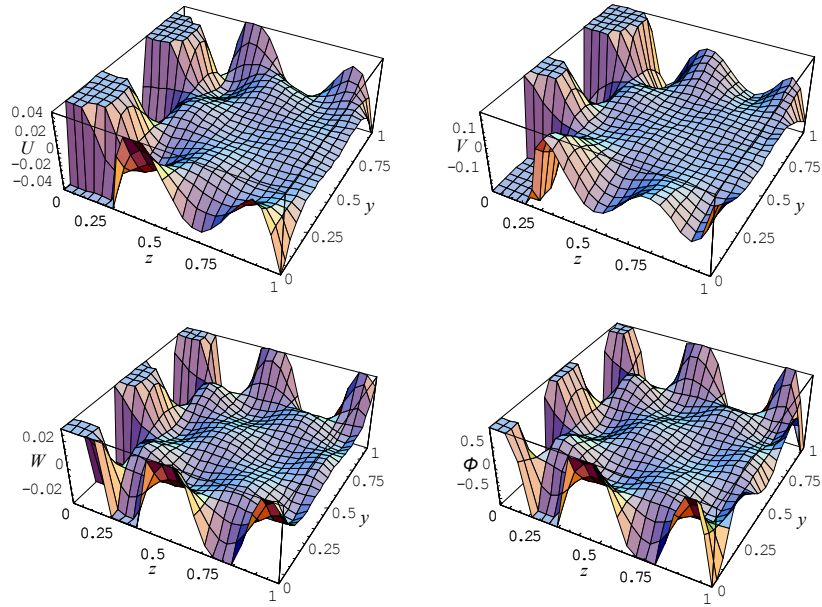


FIG. 13. Displacement and electric potential profiles of the first mode for the linearly FGPM square rod at  $kd = 60$ .

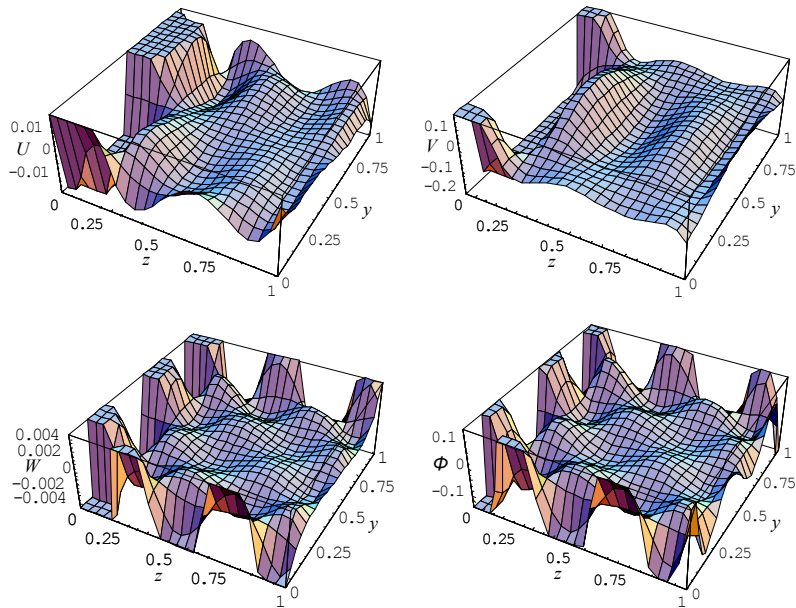


FIG. 14. Displacement and electric potential profiles of the third mode for the sinusoidally FGPM square rod at  $kd = 60$ .

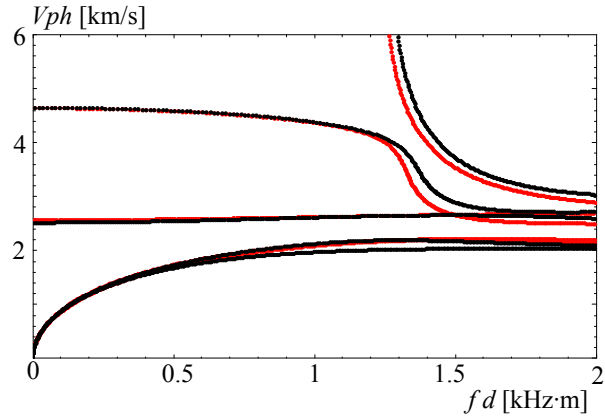


FIG. 15. Phase velocity dispersion curves for the linearly FGPM square rod; red lines:  $y$ -directional FGPM rod, black lines:  $z$ -directional FGPM rod.

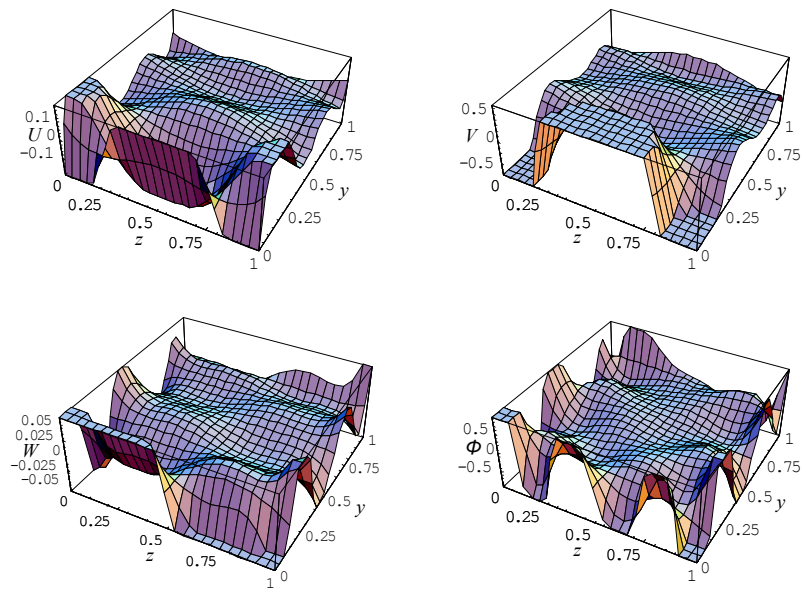


FIG. 16. Displacement and electric potential profiles of the third mode for the linearly  $y$ -directional FGPM square rod at  $kd = 60$ .

#### 4. Conclusions

In this paper, a double orthogonal polynomial approach is proposed to solve the wave propagation in a rectangular 2D FGPM rod. The dispersion curves and mechanical displacement components and electric potential distributions of

various rectangular FGPM rods are presented and discussed. According to the numerical results, we can draw the following conclusions:

a) Numerical comparison of the dispersion curves with reference solutions shows that the extended orthogonal polynomial method is appropriate to solve the guided wave propagation problem in 2D FGPM structures.

b) Both the width to height ratio and the gradient function have significant influences on the guided wave characteristics.

c) High frequency waves propagate predominantly around the side with the material having the lower wave speed.

## 5. Acknowledgment

The work was supported by the National Natural Science Foundation of China (No. 11272115) and the Outstanding Youth Science Foundation of Henan Polytechnic University (No. J2013-08), China. Jiangong Yu also gratefully acknowledges the support by the Alexander von Humboldt-Foundation (AvH) to conduct his research works at the Chair of Structural Mechanics, Faculty of Science and Technology, University of Siegen, Germany.

## References

1. C.C.M. WU, M. KAHN, W. MOY, *Piezoelectric ceramics with functional gradients: A new application in material design*, Journal of the American Ceramic Society, **79**, 3, 809–812, 1996.
2. K. TAKAGI, J.F. LI, S. YOKOYAMA, R. WATANABE, *Fabrication and evaluation of PZT/Pt piezoelectric composites and functionally graded actuators*, Journal of the European Ceramic Society, **23**, 1577–1583, 2003.
3. X. ZHU, J. ZHU, S. ZHOU, Q. LI, Z. LIU, *Microstructures of the monomorph piezoelectric ceramic actuators with functional gradients*, Sensors & Actuators A: Physical, **74**, 198–202, 1999.
4. X. LI, J.S. VARTULI, D.L. MILIUS, I.A. AKSAY, W.Y. SHIH, W.H. SHIH, *Electromechanical properties of a ceramic d31-gradient flextensional actuator*, Journal of the American Ceramic Society, **84**, 5, 996–1003, 2001.
5. J.F. LI, K. TAKAGI, M. ONO, W. PAN, R. WATANABE, *Fabrication and evaluation of porous ceramics and porosity-graded piezoelectric actuators*, Journal of the American Ceramic Society, **86**, 7, 1094–1098, 2003.
6. Y.H. CHEN, J. MA, T. LI, *A functional gradient ceramic monomorph actuator fabricated using electrophoretic deposition*, Ceramics International, **30**, 683–687, 2004.
7. J. QUI, J. TANI, T. UENO, T. MORITA, H. TAKAHASHI, H. DU, *Fabrication and high durability of functionally graded piezoelectric bending actuators*, Smart Materials and Structures, **12**, 115–121, 2003.

8. D. JIN, Z. MENG, *Functionally graded PZT/ZnO piezoelectric composites*, Journal of Materials Science Letters, **22**, 971–974, 2003.
9. G.R. LIU, J. TANI, *Characteristics of wave propagation in functionally gradient piezoelectric material plates and its response analysis. Part 1: Theory. Part 2: Calculation results*, Transactions of the Japan Society of Mechanical Engineers **57**(A), 541, 2122–2133, 1991.
10. X. HAN, G.R. LIU, *Elastic waves in a functionally graded piezoelectric cylinder*, Smart Mater. Struct., **12**, 962–971, 2003.
11. G.R. LIU, K.Y. DAI, X. HAN, T. OHYOSHI, *Dispersion of waves and characteristic wave surfaces in functionally graded piezoelectric plates*, Journal of Sound and Vibration, **268**, 131–147, 2003.
12. A. CHAKRABORTY, D. ROY MAHAPATRA, S. GOPALAKRISHNAN, *Finite element simulation of BAW propagation in inhomogeneous plate due to piezoelectric actuation*, Lecture Notes in Computer Science, 715–724, 2003.
13. A. CHAKRABORTY, S. GOPALAKRISHNAN, E. KAUSEL, *Wave propagation analysis in inhomogeneous piezo-composite layer by the thin-layer method*, Int. J. Numer. Meth. Engng, **4**, 567–598, 2005.
14. D. ROY MAHAPATRA, A. SINGHAL, S. GOPALAKRISHNAN, *Lamb wave characteristics of thickness-graded piezoelectric IDT*, Ultrasonics, **43**, 9, 736–746, 2005.
15. S.M. HASHEMINEJAD, M. ALAEI-VARNOSFADERANI, *Vibroacoustic response and active control of a fluid-filled functionally graded piezoelectric material composite cylinder*, Journal of Intelligent Material Systems and Structures, **23**, 7, 775–790, 2012.
16. X.Y. LI, Z.K. WANG, S.H. HUANG, *Love waves in functionally graded piezoelectric materials*, International Journal of Solids and Structures, **41**, 7309–7328, 2004.
17. J. LIU, Z.K. WANG, *The propagation behavior of Love waves in a functionally graded layered piezoelectric structure*, Smart Mater. Struct., **14**, 137–146, 2005.
18. L.M. GAO, J. WANG, ZH. ZHONG, J.K. DU, *An analysis of surface acoustic wave propagation in functionally graded plates with homotopy analysis method*, Acta Mechanica, **208**, 249–258, 2009.
19. J.E. LEFEBVRE, V. ZHANG, J. GAZALET, T. GRYBA, V. SAUDANE, *Acoustic wave propagation in continuous functionally graded plates: an extension of the Legendre polynomial approach*, IEEE Trans. Ultras. Ferr. R Freq. Control, **48**, 1332–1339, 2001.
20. Y. JIANGONG, W. BIN, C. GUOQIANG, *Wave characteristics in functionally graded piezoelectric hollow cylinders*, Archive of Applied Mechanics, 2009, **79**, 9, 807–824, 2009.
21. J.K. DU, X.Y. JIN, J. WANG, K. XIAN, *Love wave propagation in functionally graded piezoelectric material layer*, Ultrasonics, **46**, 1, 13–22, 2007.
22. S. DATTA, B.J. HUNSINGER, *Analysis of surface waves using orthogonal functions*, J. Appl. Phys., **49**, 2, 475–479, 1978.
23. T. HAYASHI, W.-J. SONG, J. L. ROSE, *Guided wave dispersion curves for a bar with an arbitrary cross-section, a rod and rail example*, Ultrasonics, **41**, 175–183, 2003.

Received June 18, 2014; revised version March 24, 2015.